Shape of thermal plumes in a compressible mantle with depth-dependent viscosity

Wei Leng[1] and Michael Gurnis[1]

Received 18 January 2012; revised 14 February 2012; accepted 16 February 2012; published 13 March 2012.

[1] The mantle plume model has been invoked to explain the formation of large igneous provinces (LIP) and associated age-progressive hotspot tracks. The shape of mantle plumes should be significantly altered by physical properties of the mantle and will influence how plume theory is used to interpret observational constraints. Based on theoretical analysis and numerical modeling, we explore the parameters that control the shape of thermal plumes in a compressible mantle. A theoretical analysis shows that the ambient mantle viscosity plays a dominant role in determining the radius of thermal plumes. This analysis is verified by numerical solutions. A continuously decreasing mantle viscosity from the CMB to the lithosphere can effectively reduce the radius of both plume head and tail. A low viscosity zone between 100 and 660 km depths where viscosity decreases by a factor of 100 reduces the radius of a plume conduit by approximately a factor of 3. Such a low viscosity zone can reduce the plume head radius impinging the lithosphere from larger than 500 km to ~200 km. When the low viscosity zone is confined to between 100 and 410 km depths, the plume head size becomes even smaller. To form large igneous provinces, a small plume head implies time-progressive volcanism from LIP center to LIP edge. **Citation:** Leng, W., and M. Gurnis (2012), Shape of thermal plumes in a compressible mantle with depth-dependent viscosity, *Geophys. Res. Lett.*, *39*, L05310, doi:10.1029/2012GL050959.

1. Introduction

[2] Mantle plumes originate from the deep interior, possibly at the core-mantle boundary (CMB), from thermal instabilities, and rise through the whole mantle and impinge the bottom of the lithosphere to form hotspots [*Morgan*, 1971]. A conventional plume model consists of a mushroom-shaped plume head and a thin plume tail conduit [*Richards et al.*, 1989; *Campbell and Griffiths*, 1990; *Griffiths and Campbell*, 1990; *Coffin and Eldholm*, 1994; *Campbell*, 2007]. When the large plume head reaches the base of the lithosphere, its high temperature may generate extensive melting and massive basaltic eruptions, a process used to interpret the formation of large igneous provinces (LIPs) [*Richards et al.*, 1989, 1991; *Ernst and Buchan*, 2002; *Campbell*, 2007]. The remaining plume tail conduit continues to impinge the lithosphere leading to age-progressive volcanism (hotspot tracks) that follow LIPs [*Davies*, 1988; *Richards et al.*, 1989; *Sleep*, 1990; *Coffin and Eldholm*, 1994; *Campbell*, 2007].

[3] The shape of mantle plumes during generation and ascent has been studied though laboratory experiments and numerical modeling [*Campbell and Griffiths*, 1990; *Griffiths and Campbell*, 1990; *van Keken*, 1997; *Wullner and Davies*, 1999]. These studies consider the mantle as incompressible and isoviscous or with temperature-dependent viscosity. Different from the incompressible studies, in a compressible mantle, the density and plume excess temperature are controlled by mantle compressibility and both vary with depths [*Leng and Zhong*, 2008]. Moreover, the viscosity in the mantle is not only temperature-dependent, but also depth-dependent [e.g., *Mitrovica and Forte*, 2004]. Long wavelength geoid anomalies over subduction zones and hotspots imply an upper mantle with a reduced viscosity compared to the lower mantle [*Richards et al.*, 1988; *Hager and Richards*, 1989]. Previous models have shown that this low viscosity layer leads to a narrowing of the plume in the upper mantle [*Richards et al.*, 1988; *Farnetani and Richards*, 1994]. However, the combination effects of mantle density, plume excess temperature and ambient mantle viscosity on the plume shape in a compressible mantle have not been quantified. Due to the poor resolution of the viscosity structure in the upper mantle [*Mitrovica and Forte*, 2004; *Paulson and Richards*, 2009], it is also essential to investigate how the different thickness and viscosity reduction ratio of the low viscosity layer in the upper mantle influences shape of plumes.

[4] Using a 2-D axisymmetric compressible mantle convection model, we investigate the combined effects of mantle compressibility, plume excess temperature, coefficient of thermal expansion and depth-dependent viscosity on the shape of mantle plumes. We only consider thermal plumes, although thermo-chemical plumes may have a more complicated range of shapes as shown by *Farnetani and Samuel* [2005]. We first develop an analytic model that embodies the critical parameters controlling the shape of a mantle plume. Then we confirm our theoretical analysis with numerical modeling. Finally we discuss the implication of these results for the seismic detection of mantle plumes and for the formation processes of LIPs.

2. Plume Shape in a Compressible Mantle With Depth-Dependent Viscosity

[5] For a plume conduit rising in a compressible mantle, we obtain the balance between buoyancy and viscous forces. Over a unit vertical distance, the buoyancy force F_b and the viscous force F_v can be expressed as

$$F_b = \rho\alpha\Delta T g \pi r^2, \tag{1}$$

$$F_v = \frac{V}{r}\eta \cdot 2\pi r = 2\pi V\eta, \tag{2}$$

[1]Seismological Laboratory, California Institute of Technology, Pasadena, California, USA.

Copyright 2012 by the American Geophysical Union.
0094-8276/12/2012GL050959

where ρ, α, ΔT, g, r, V and η are the density, coefficient of thermal expansion, plume excess temperature (i.e., temperature difference between plume and the ambient mantle), gravitational acceleration, plume radius, plume ascent velocity at plume center and ambient mantle viscosity, respectively. Let $F_b = F_v$, we have

$$V = \frac{\rho\alpha\Delta T g r^2}{2\eta}. \tag{3}$$

If we assume there is no material exchange between the plume conduit and the ambient mantle during plume ascent (supported numerically [*Leng and Zhong*, 2008]), we have the conservation of mass flux for the plume conduit

$$\rho\pi r^2 V = C_1, \tag{4}$$

where C_1 is an arbitrary constant that can be determined through numerical experiments. Combining equations (3) and (4), we have

$$\frac{\rho^2\alpha\Delta T g\pi r^4}{2\eta} = C_1. \tag{5}$$

Consequently, at two different depth z_1 and z_2, the ratio of plume radii is

$$\frac{r_1}{r_2} = \left(\frac{\rho_2^2\Delta T_2\alpha_2\eta_1}{\rho_1^2\Delta T_1\alpha_1\eta_2}\right)^{0.25}. \tag{6}$$

From equation (6), the ratio of the radius of plume conduit at two different depths can be computed given the depth distribution of background density, plume excess temperature, coefficient of thermal expansion and ambient mantle viscosity.

[6] The ratio of plume excess temperature at depths z_1 and z_2 can be expressed as [*Leng and Zhong*, 2008]

$$\frac{\Delta T_2}{\Delta T_1} = e^{\bar{\alpha}D_i(z_2 - z_1)}, \tag{7}$$

where $\bar{\alpha}$ is the averaged coefficient of thermal expansion over depth z_1 to z_2, $\bar{\alpha} = \frac{\int_{z_1}^{z_2}\alpha dz}{z_2 - z_1}$; $D_i = \frac{\alpha g d}{c_p}$, is the dissipation number where d and C_p are the mantle thickness and heat capacity at constant pressure, respectively. All values in (7) are nondimensional (see *Leng and Zhong* [2008] for details).

[7] From equation (6), the plume radius is proportional to viscosity to the power 0.25, but inversely proportional to the coefficient of thermal expansion and plume excess temperature to the power 0.25. The plume radius is also inversely proportional to mantle density to the power 0.5. The derivation of equation (6) does not consider the effect of chemical buoyancy therefore this equation is only applicable to thermal plumes.

3. Numerical Modeling and Results

3.1. Model Setup

[8] We use a 2-D axisymmetric convection model (the governing equation and model details are given by *Leng and Zhong* [2010]), to determine the shape of plumes in a compressible mantle where both adiabatic and viscous heating are considered. The model dimensions are 1435 km in radial distance by 2870 km in depth. The Rayleigh and dissipation numbers are 1×10^7 and 1.15, respectively, which are close to the estimation of actual mantle conditions. We have 257×257 numerical grids for the model domain. The top and bottom boundaries are both free-slip. The coefficient of thermal expansion decreases by a factor of 5 from the surface to the CMB. We use the Adams-Williamson equation of state [*Birch*, 1952]. The density of the mantle increases by a factor of 1.65 from the surface to the CMB. The initial background temperature field consists of an adiabatic profile with top and bottom thermal boundary layers of 100 km thickness, the same as that used by *Leng and Zhong* [2010].

[9] We use a viscosity η that is temperature- and depth-dependent:

$$\eta(T, z) = \eta_r(z)\exp[-E_a(T - T_{adi}(z))], \tag{8}$$

where T and z are temperature and depth; $\eta_r(z)$ is the depth-dependent viscosity profile; $T_{adi}(z)$ is an adiabatic temperature profile, the same as the initial temperature; The activation energy E_a is chosen to give a temperature-induced viscosity contrast of 10^6. The depth-dependent viscosity structure will be discussed below.

[10] A plume is induced by slightly perturbing the bottom thermal boundary layer at the center of the domain. To quantify the plume radius at each depth, the plume region is defined as the area where the temperature T is larger than a threshold:

$$T > T_{ave} + f(T_c - T_{ave}), \tag{9}$$

where T_{ave} and T_c are the horizontally averaged temperature and centerline temperature, respectively; f is a constant 0.1. We will justify our choice of f below.

3.2. Plume Shape With Continuously Varying Viscosity

[11] With a case with no depth-dependent viscosity, case A01, the plume is generated from CMB, ascends through the whole mantle, and impinges the bottom of the lithosphere (Figure 1a). The temperature and velocity fields show that the hot layer at the base keeps feeding the plume with lateral flow towards the centerline (Figure 1a). To better visualize the plume, we show the residual temperature for case A01 (Figure 1b), i.e., the temperature after the horizontally averaged temperature is subtracted. The mantle density increases by 1.65 from the surface to the CMB (Figure 2a). Both mantle temperature and plume (centerline) temperature increase with depth (Figure 2a). It can be observed that plume excess temperature decreases from ~1000 K at the CMB to ~400 K beneath the lithosphere (Figure 1b), as predicted by equation (7) [*Leng and Zhong*, 2008]. During its ascent, the plume head expands to a radius of 600 km before impinging and flattening beneath the lithosphere (Figure 1b). This scenario is similar to the conventional plume scenario [*Campbell and Griffiths*, 1990; *Coffin and Eldholm*, 1994; *Campbell*, 2007]. After the last stage of evolution shown in Figure 1b, the thermal structure of plume conduit varies little with time. So, based on equation (9), we quantify the radius of plume conduit at each depth between 2570 km and 287 km for the last stage of evolution. When mantle viscosity is independent of depth for case A01 (Figure 2b), the radius of plume tail does not vary significantly with depth (Figure 2c).

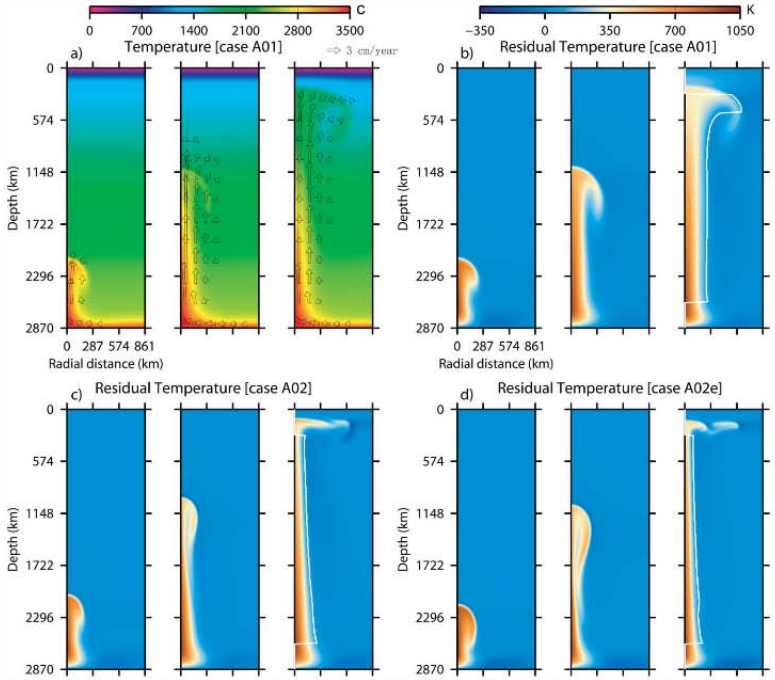

Figure 1. (a) The temperature and velocity at different stages of plume evolution for case A01. (b) The corresponding residual temperature (i.e., the temperature after the horizontally averaged temperature is subtracted) for case A01. Residual temperatures for cases (c) A02 and (d) A02e during their plume evolutionary processes. For each case, the white line in the last residual temperature field shows the detected plume boundary. Notice that our actual model dimension is 1435 km by 2870 km. Here only the middle part of our model is shown.

[12] We then add a depth-dependent viscosity for case A02, in which the ambient mantle viscosity continuously decreases by a factor of 100 from 2570 to 100 km depth (Figure 2b). The plume head size during ascent is smaller compared with case A01 due to the viscosity reduction (Figure 1c). At the last stage of evolution shown in Figure 1c, the quantified plume tail radius decreases significantly from bottom to top of the mantle (Figure 2c, case A02 with $f = 0.1$). At 2570 and 500 km depths, plume radius is 246 and 106 km, respectively; the plume radius decreases by a factor of 2.3.

[13] Based on equation (6), the observed plume radius variation with depth for case A02 can be theoretically explained. For z_1 and z_2 at 2570 and 500 km depths, we have $\rho_1/\rho_2 = 1.43$, $\alpha_1/\alpha_2 = 0.33$, $\Delta T_1/\Delta T_2 = 2.2$. These values are not affected by depth-dependent viscosity. We then obtain from equation (6)

$$\frac{r_1}{r_2} = 0.9 * \left(\frac{\eta_1}{\eta_2}\right)^{0.25}. \tag{10}$$

From equation (10), the variation of plume radius can be computed from ambient mantle viscosity contrast. For case A01, with no depth-dependent viscosity variation, we expect plume radius to increase slightly from the CMB to the surface by ~10%. Numerical results show this slight increase of plume radius (Figure 2c), excluding the shallow depth portion where plume head expands beneath the lithosphere. For case A02, $\eta_1/\eta_2 = 45$ (Figure 2b), equation (10) predicts a decrease of plume radius of a factor of 2.3, equal to our numerical results. The agreement between our numerical results and theoretical analysis indicates that our theoretical model works well.

[14] To choose an appropriate f value in equation (9), we quantify the plume heat flux for case A02 with different f values. The plume heat flux Q_p is defined as

$$Q_p = \int_{R_p(f=f_0)} \rho C_p u (T - T_{ave}) \cdot 2\pi r dr, \tag{11}$$

where C_p is the specific heat which is taken as 1000 J/(kg K); u is the vertical velocity. The integration range R_p is the detected plume area with f set to be f_0. When f is 0.0, all the regions with temperature higher than the average temperature are detected as plume area (Figure 2c). The plume heat flux for this single plume decreases from 3×10^{11} W at the CMB to 1.6×10^{11} TW at the surface (Figure 2d), as predicted by *Leng and Zhong* [2008]. When f increases from 0.0 to 0.1, the plume radius decreases significantly at all depths (Figure 2c), whereas the plume heat flux only slightly decreases (Figure 2d). This indicates that by increasing f to 0.1, we exclude a broad region with positive

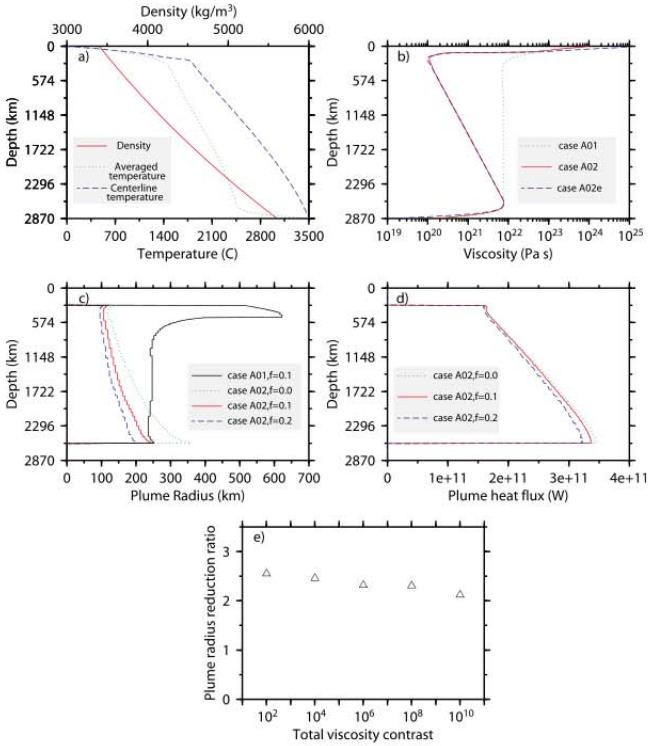

Figure 2. (a) Mantle density profile, averaged temperature and centerline temperature for case A01 at the last evolutionary stage shown in Figure 1a. (b) The viscosity structure for cases A01, A02 and A02e. (c) The detected plume radius for cases A01 and A02. For case A02, we also show the effects of varying *f* on the detected plume radius. (d) The plume heat flux for case A02 with different *f*. (e) The plume radius reduction ratios (i.e., the ratio of plume radius at 2570 km depth to plume radius at 500 km depth) for cases A02 and A02b-A02e with different viscosity contrasts in response to different activation energies.

temperature anomaly but only small upward velocities. When *f* is further increased to 0.2, both plume radius and plume heat flux decrease moderately (Figures 2c and 2d), indicating parts of hot upwelling are excluded. To preserve most of the plume heat flux while excluding a large region with positive temperature anomaly but small upward velocities, we consider $f = 0.1$ is an appropriate value for defining a plume.

[15] The activation energy of the mantle can be large and may lead to viscosity contrast of ten or more orders of magnitude (from only temperature) [*Karato and Wu*, 1993]. We compute a series of cases A02b-A02e which are similar to case A02 but with different activation energies so that the total viscosity contrast varies from 10^2 to 10^{10}. The activation energy affects the size of plume head. For case A02e with total viscosity contrast of 10^{10} (Figure 2b), the plume head size is much larger than case A02 (Figure 1d). However, the reduction ratio of plume radius from 2570 to 500 km depth is only slightly affected by the activation energy (Figure 2e). For all the five cases, the plume radius reduction ratios are close to 2.3 which agree well with our theoretical analysis.

3.3. Plume Shape With a Low Viscosity Layer in the Upper Mantle

[16] It has been shown that there is a low viscosity layer in the upper mantle where viscosity could decrease by a factor of 30□100 or even larger [*Richards et al.*, 1988; *Hager and Richards*, 1989; *Moresi and Gurnis*, 1996; *Mitrovica and Forte*, 2004]. However, the thickness and viscosity reduction in this layer remain largely uncertain [*Mitrovica and Forte*, 2004; *Paulson and Richards*, 2009]. Here we explore the effects of a low viscosity layer with different thickness and viscosity on the plume shape.

[17] Compared to the background case with no depth-dependent viscosity, A01, we now include a low viscosity layer in the upper mantle between 100 and 660 km depths for case B01 (Figure 3a). The ambient mantle viscosity decreases by a factor of 100 from the lower to the upper mantle (Figure 3c). The ascending velocity of the plume increases abruptly at 660 km depth (Figure 3c) when plume radius is significantly reduced by this viscosity discontinuity (Figure 3a). We compare plume radii at 660 and 410 km depths (white line, Figure 3a). The results show that plume radius decreases by a factor of 3.0 for case B01. If the

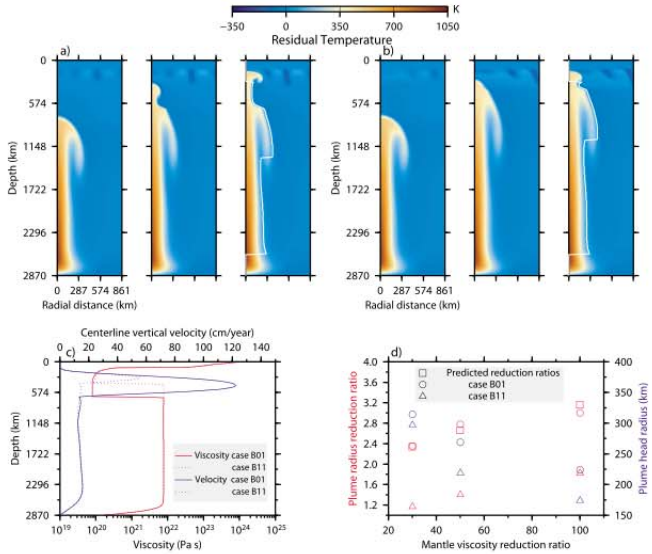

Figure 3. (a and b) Residual temperatures for cases B01 and B11, respectively. For each case, the white line in the last residual temperature field shows the plume boundary. (c) The viscosity profile and centerline vertical velocity for cases B01 and B11 at the last evolutionary stage shown in Figures 3a and 3b. (d) Red symbols show the theoretical predictions (squares) and numerical results of the plume radius reduction ratios for case B01 with a low viscosity layer between 100□660 km depths (circles) and for case B11 with a low viscosity layer between 100□410 km depths (triangles). Blue symbols show the corresponding plume head radius when plume impinges the bottom of the lithosphere.

viscosity reduction ratio at 660 km depth is reduced from 100 to 50, the plume radius reduction ratio decreases from 3.0 to 2.8 (Figure 3d). A further decrease of viscosity reduction ratio to 30 leads to a plume radius reduction ratio of 2.4 (Figure 3d).

[18] These results can also be explained by equation (6). The density, plume excess temperature and coefficient of thermal expansion vary little across the viscosity discontinuity at 660 km depth, therefore equation (6) becomes,

$$\frac{r_1}{r_2} = \left(\frac{\eta_1}{\eta_2}\right)^{0.25}. \tag{12}$$

The theoretical prediction for the plume radius reduction can then be computed based on viscosity variation at 660-km discontinuity. Our theoretical results agree with numerical results (Figure 3d).

[19] We further test another case B11 with a low viscosity layer between 100 and 410 km depths (Figure 3b), where ambient mantle viscosity decreases by a factor of 100 (Figure 3c). The ascending velocity of the plume also increases at viscosity discontinuity, but not as significant as for case B01 (Figure 3c). Plume radius decreases by a factor of 1.8 from 410 to 330 km depth. This ratio is much smaller than the theoretical prediction of 3.2 (Figure 3d). This discrepancy is likely caused by the plume reaching the bottom of the lithosphere where horizontal advection dominates before it has fully adjusted after passing the viscosity discontinuity at 410 km depth (Figure 3b). When the viscosity reduction ratio at 410 km depth are reduced from 100 to 30 for case B11, it becomes more obvious that a thinner low viscosity layer has less effects to narrow the plume radius (Figure 3d). For a viscosity reduction ratio of 30 at 410 km depth, the plume radius only decreases by a factor of 1.2 (Figure 3d). The narrowing effect becomes almost negligible.

[20] With a strong viscosity contrast between the lower and the upper mantle, the shape of a plume head is quite different from a traditional plume model. Compared with case A01 (Figure 1b), the size of plume head is much smaller for case B01 and B11 when the plume reaches the bottom of the lithosphere (Figures 3a and 3b). We define the plume head size impinging the lithosphere as following. When plume excess temperature at 150 km depth becomes 350 K or higher, we consider that partial melting and surface volcanic eruption begin. The maximum plume radius between 150 and 330 km depths at this time is defined as plume head size impinging the lithosphere. For case B01, the plume head size decreases with increased viscosity reduction ratio at 660 km depth (Figure 3d). If viscosity decreases by a factor of 100 at 660 km depth, the plume head size impinging the lithosphere is just 225 km. With a thinner low viscosity layer between 100 and 410 km depths (case B11), the plume head size becomes even smaller, 175 km when viscosity reduction ratio is 100 (Figure 3d). Therefore, although a thinner low viscosity layer has less effect on narrowing the plume, it does cause a smaller plume head impinging the lithosphere. This is because a thinner low viscosity layer limits the distance for the plume head to

expand after it penetrates the viscosity discontinuity (comparing Figures 3a and 3b).

4. Discussion and Conclusion

[21] From our results, the shape of mantle plume at different depths can be predicted from contrasts in ambient mantle viscosity. This can inform us on our ability to seismically detect plumes. *Sun et al.* [2010] proposed that a narrow mid-mantle plume with diameter less than 150 km exists below southern Africa. If such a narrow plume penetrates to the surface, a viscosity reduction ratio of 100 at 660 km depth would lead to plume radius reduction ratio of ~3.0 (Figure 3d). Therefore the plume diameter in the upper mantle would only be ~50 km. Such a small plume can hardly be detected with current seismic tomography studies [i.e., *Montelli et al.*, 2004], which may explain why there is no seismic anomalies detected in the upper mantle beneath some hotspots. On the other hand, if the plume diameter estimated in the upper mantle is up to 140 km, e.g., the Hawaii hotspot [*Zhong and Watts*, 2002], we expect to observe a large plume conduit with a diameter of 420 km in the lower mantle. Such a large plume conduit can be a target for future plume detection with advanced seismic techniques.

[22] Our results also have important implications for the formation process of large igneous provinces. With a low viscosity upper mantle between 100 and 660 km depths where viscosity decreases by a factor of 100, plume head radius is reduced from larger than 500 km to ~220 km. A thinner low viscosity layer between 100 and 410 km depths leads to an even smaller plume head radius of 175 km (Figure 3d). From geological observations, the size of the LIPs can be as large as 1000 km in radius and LIPs are typically formed within several million years [*Ernst and Buchan*, 2002]. If these LIPs are formed by plume head impinging the lithosphere, a small plume head of ~200 km in radius suggests that the lateral flow velocity of plume materials in the asthenosphere should be quite large, up to several tens of cm/year. The details of lateral flow of plume material in the asthenosphere have been investigated [*Sleep*, 1996]. Given these strong lateral flows, we make a geologically testable prediction that the volcanic rock sequences in a LIP should show a prominent age-progressive pattern from its center to its edge. Such a pattern could be detectable with precise age-dating techniques.

[23] We did not consider subadiabatic temperature effect, up to 200 K [*Leng and Zhong*, 2010]. Since plume radius is proportional to plume excess temperature to the power 0.25, a subadibatic temperature of <200 K should have minor effects on plume shape.

[24] In conclusion, we develop a theoretical analysis for predicting plume shape variation in a compressible mantle. Our analysis shows that the ambient mantle viscosity variation plays a dominant role in determining the radius of thermal plumes. This analysis is confirmed by numerical modeling results. A viscosity reduction of a factor of 100 in the upper mantle reduces plume radius by approximately a factor of 3. Such a viscosity reduction also effectively reduces the plume head radius impinging the lithosphere from larger than 500 km to ~220 km. If the low viscosity upper mantle is confined to be between 100 and 410 km depths, the plume head size becomes even smaller, ~175 km in radius. To form large igneous provinces, a small plume head size implies a prominent age-progressive volcanic pattern from the center of a LIP to its edge, which should be detectable from advanced age-dating techniques.

[25] **Acknowledgments.** We thank Norm Sleep and an anonymous reviewer for their constructive reviews which significantly improved this paper. WL was supported by O. K. Earl Fellowship, and NSF grants EAR-0810303 and EAR-0855815.

[26] The Editor thanks Norman H. Sleep and an anonymous reviewer for their assistance in evaluating this paper.

References

Birch, F. (1952), Elasticity and constitution of the Earth's interior, *J. Geophys. Res.*, *57*, 227–286, doi:10.1029/JZ057i002p00227.

Campbell, I. H. (2007), Testing the plume theory, *Chem. Geol.*, *241*, 153–176, doi:10.1016/j.chemgeo.2007.01.024.

Campbell, I. H., and R. W. Griffiths (1990), Implications of mantle plume structure for the evolution of flood basalts, *Earth Planet. Sci. Lett.*, *99*, 79–93, doi:10.1016/0012-821X(90)90072-6.

Coffin, M. F., and O. Eldholm (1994), Large igneous provinces: Crustal structure, dimensions, and external consequences, *Rev. Geophys.*, *32*(1), 1–36, doi:10.1029/93RG02508.

Davies, G. F. (1988), Oceanic bathymetry and mantle convection: 1. Large-scale flow and hotspots, *J. Geophys. Res.*, *93*, 10,467–10,480, doi:10.1029/JB093iB09p10467.

Ernst, R. E., and K. L. Buchan (2002), Maximum size and distribution in time and space of mantle plumes: Evidence from large igneous provinces, *J. Geodyn.*, *34*, 309–342, doi:10.1016/S0264-3707(02)00025-X.

Farnetani, C. G., and M. A. Richards (1994), Numerical investigations of the mantle plume initiation model for flood basalt events, *J. Geophys. Res.*, *99*, 13,813–13,833, doi:10.1029/94JB00649.

Farnetani, C. G., and H. Samuel (2005), Beyond the thermal plume paradigm, *Geophys. Res. Lett.*, *32*, L07311, doi:10.1029/2005GL022360.

Griffiths, R. W., and I. H. Campbell (1990), Stirring and structure in mantle starting plumes, *Earth Planet. Sci. Lett.*, *99*, 66–78, doi:10.1016/0012-821X(90)90071-5.

Hager, B. H., and M. A. Richards (1989), Long-wavelength variations in Earth's geoid: Physical models and dynamical implications, *Philos. Trans. R. Soc. London, Ser. A*, *328*, 309–327, doi:10.1098/rsta.1989.0038.

Karato, S.-I., and P. Wu (1993), Rheology of the upper mantle: A synthesis, *Science*, *260*, 771–778, doi:10.1126/science.260.5109.771.

Leng, W., and S. J. Zhong (2008), Controls on plume heat flux and plume excess temperature, *J. Geophys. Res.*, *113*, B04408, doi:10.1029/2007JB005155.

Leng, W., and S. J. Zhong (2010), Surface subsidence by mantle plume and volcanic loading in large igneous provinces, *Earth Planet. Sci. Lett.*, *291*, 207–214, doi:10.1016/j.epsl.2010.01.015.

Mitrovica, J. X., and A. M. Forte (2004), A new inference of mantle viscosity based upon joint inversion of convection and glacial isostatic adjustment data, *Earth Planet. Sci. Lett.*, *225*, 177–189, doi:10.1016/j.epsl.2004.06.005.

Montelli, R., G. Nolet, F. A. Dahlen, G. Masters, E. R. Engdahl, and S.-H. Hung (2004), Finite-frequency tomography reveals a variety of plumes in the mantle, *Science*, *303*, 338–343, doi:10.1126/science.1092485.

Moresi, L., and M. Gurnis (1996), Constraints on the lateral strength of slabs from three-dimensional dynamic flow models, *Earth Planet. Sci. Lett.*, *138*, 15–28, doi:10.1016/0012-821X(95)00221-W.

Morgan, W. (1971), Convection plumes in the lower mantle, *Nature*, *230*, 42–43, doi:10.1038/230042a0.

Paulson, A., and M. A. Richards (2009), On the resolution of radial viscosity structure in modeling long-wavelength postglacial rebound data, *Geophys. J. Int.*, *179*(3), 1516–1526, doi:10.1111/j.1365-246X.2009.04362.x.

Richards, M. A., B. H. Hager, and N. H. Sleep (1988), Dynamically supported geoid highs over hotspots: Observation and theory, *J. Geophys. Res.*, *93*, 7690–7708, doi:10.1029/JB093iB07p07690.

Richards, M. A., R. A. Duncan, and V. E. Courtillot (1989), Flood basalts and hot-spot tracks: Plume heads and tails, *Science*, *246*, 103–107, doi:10.1126/science.246.4926.103.

Richards, M. A., D. L. Jones, R. A. Duncan, and D. J. Depaolo (1991), A mantle plume initiation model for the Wrangellia flood basalt and other oceanic plateaus, *Science*, *254*, 263–267, doi:10.1126/science.254.5029.263.

Sleep, N. H. (1990), Hotspots and mantle plumes: Some phenomenology, *J. Geophys. Res.*, *95*, 6715–6736, doi:10.1029/JB095iB05p06715.

Sleep, N. H. (1996), Lateral flow of hot plume material ponded at sublithospheric depths, *J. Geophys. Res.*, *101*, 28,065–28,083, doi:10.1029/96JB02463.

Sun, D., D. Helmberger, and M. Gurnis (2010), A narrow, mid-mantle plume below southern Africa, *Geophys. Res. Lett.*, *37*, L09302, doi:10.1029/2009GL042339.

van Keken, P. (1997), Evolution of starting mantle plumes: A numerical and laboratory comparison between models, *Earth Planet. Sci. Lett.*, *148*, 1–11, doi:10.1016/S0012-821X(97)00042-3.

Wullner, U., and G. F. Davies (1999), Numerical evaluation of mantle plume spacing, size, flow rates and unsteadiness, *J. Geophys. Res.*, *104*, 7377–7387, doi:10.1029/1998JB900094.

Zhong, S. J., and A. B. Watts (2002), Constraints on the dynamics of mantle plumes from uplift of the Hawaiian Islands, *Earth Planet. Sci. Lett.*, *203*, 105–116, doi:10.1016/S0012-821X(02)00845-2.

M. Gurnis and W. Leng, Seismological Laboratory, California Institute of Technology, 1200 E. California Blvd., Pasadena, CA 91125, USA. (leng@caltech.edu)